Wu *et al. Soft Sci* 2024;4:42
DOI: 10.20517/ss.2024.51

Soft Science

Research Article

Open Access

Check for updates

Dual magnetic particles modified carbon nanosheets in CoFe/Co@NC heterostructure for efficient electromagnetic synergy

Zhanming Wu[#], Jun Huang[#], Xiaojun Zeng[*]

Jiangxi Key Laboratory of Advanced Ceramic Materials, School of Materials Science and Engineering, Jingdezhen Ceramic University, Jingdezhen 333403, Jiangxi, China.
[#]Authors contributed equally.

[*]**Correspondence to:** Prof. Xiaojun Zeng, Jiangxi Key Laboratory of Advanced Ceramic Materials, School of Materials Science and Engineering, Jingdezhen Ceramic University, Rixin Road, Fuliang County, Jingdezhen 333403, Jiangxi, China. E-mail: zengxiaojun@jcu.edu.cn

How to cite this article: Wu Z, Huang J, Zeng X. Dual magnetic particles modified carbon nanosheets in CoFe/Co@NC heterostructure for efficient electromagnetic synergy. *Soft Sci* 2024;4:42. https://dx.doi.org/10.20517/ss.2024.51

Received: 9 Oct 2024 **First Decision:** 9 Nov 2024 **Revised:** 21 Nov 2024 **Accepted:** 28 Nov 2024 **Published:** 30 Nov 2024

Academic Editor: Zhigang Chen **Copy Editor:** Pei-Yun Wang **Production Editor:** Pei-Yun Wang

Abstract

Dual magnetic particles-modified carbon materials have great potential in terms of ultrathin thickness (≤ 2 mm) and super electromagnetic wave (EMW) absorption (≤ -70 dB). Herein, using CoFe-metal-organic framework (MOF)-derived CoFe/Co@NC heterostructures composed of hollow CoFe nanospheres, solid Co nanospheres, and nitrogen-doped carbon (NC) nanosheets, we demonstrate how the dual magnetic particles regulate the electromagnetic response behavior of the heterostructure and thus steer the efficient EMW absorption performance. That is, CoFe/Co@NC heterostructure inherits an ultra-strong reflection loss (R_L) of -73.8 dB at 1.78 mm. The effective absorption bandwidth (EAB) value is also available up to 5.4 GHz. Moreover, computer simulation technology (CST) simulations reveal the good radar stealth effect of heterostructures. Experimentally, the outstanding EMW absorption of CoFe/Co@NC heterostructure is due to a large number of heterointerfaces, good conductive networks and dual magnetic nanoparticles, which bring considerable interface polarization, conduction loss, and magnetic loss characteristics. These findings underscore the importance of electromagnetic synergy induced by dual magnetic particles for steering the electromagnetic response of EMW absorbers.

Keywords: Dual magnetic particles, CoFe/Co@NC heterostructure, electromagnetic synergy, ultrathin thickness, electromagnetic wave absorption

INTRODUCTION

As electronic information technology and devices continue to advance, people's living standards have been greatly improved. Nevertheless, the presence of electromagnetic waves (EMWs) is pervasive in everyday life[1-4]. The problems of electromagnetic pollution are worsening, affecting not only people's health but also the operation of precision electronic instruments[5-7]. Meanwhile, military equipment such as stealth aircraft, radar, and precision-guided weapons urgently need to be developed[8-10]. So, outstanding EMW absorbing materials have important practical value. Among them, crafting ultra-thin absorbers that possess significant reflection attenuation and a broad frequency range remains an ongoing challenge[11]. Among various strategies, the combination of magnetic particles (iron, cobalt, nickel) and carbon materials [graphene, carbon nanotubes (CNTs), porous carbon] can obtain electromagnetic synergistic composite materials, improve impedance matching, and enhance absorption of incident EMWs[12]. However, dual magnetic ion-modified carbon-based materials face challenges in achieving efficient EMW absorption[13].

Metal-organic frameworks (MOFs) are porous crystal materials formed by the coordination of metal ions and organic groups[14], so they can be transformed into magnetic-carbon composites, while bringing about magnetic loss and dielectric loss. Furthermore, MOF derivatives also have the characteristics of high dispersion, which can uniformly disperse metal particles into the carbon matrix to form rich heterogeneous interfaces, significantly enhancing interface polarization, thereby improving EMW absorption performance[15,16]. For example, Wen *et al.* developed MOF-derived one-dimensional CNTs-modified Co/C composites with strong magnetic losses[17]. Jin *et al.* designed MOF-derived Ni@nitrogen-doped carbon (NC) hexagonal nanosheets to obtain electromagnetic synergistic absorbers[18]. However, achieving efficient EMW absorption at ultrathin thickness is still extremely challenging. Recent studies have shown that dual magnetic particles-modified carbon-based materials can bring stronger magnetic attenuation and promote impedance matching properties, which are anticipated to obtain strong EMW absorption performance at ultrathin thickness. For instance, Zhu *et al.* synthesized bimetallic composition Cu/NC@Co/NC complex materials, with a reflection loss (R_L) of -54.13 dB at a thickness of 3 mm[19]. Wang *et al.* synthesized magnetic CoFe alloy@C nanocomposites; at a thickness of 3mm, the R_L registers at -40 dB[20]. Apparently, dual magnetic particles-modified carbon materials have great potential in terms of ultrathin thickness (≤ 2 mm) and super EMW absorption (≤ -70 dB).

Herein, dual magnetic particles (hollow CoFe alloy nanospheres and solid Co nanospheres)-modified NC nanosheets are prepared by a simple chemical precipitation method and pyrolysis process. NC nanosheets embedded with CoFe alloys and metallic Co nanospheres realize abundant heterogeneous interfaces. The larger number of NC nanosheets provides opportunities for multiple reflections and scattering. Moreover, computer simulation technology (CST) simulations confirm the low radar cross section (RCS) of the CoFe/Co@NC. Therefore, the CoFe/Co@NC heterostructure inherits outstanding EMW absorption capabilities, achieving an exceptionally high R_L of -73.8 dB at a minimal thickness of 1.78 mm for optimal impedance matching. At the same time, the effective absorption bandwidth (EAB) can also reach up to 5.4 GHz.

EXPERIMENTAL

Synthesis of CoFe/Co@NC heterostructure

Cobalt nitrate hexahydrate (1.6 mmol) and ferrous sulfate heptahydrate (0.7 mmol) were dissolved in 20 mL of deionized water. Additionally, 2-Methylimidazole (4 mmol) was mixed with 60 mL of deionized water, which was subsequently poured into the mixture prepared in the previous step. The obtained mixture was agitated at ambient temperature for a duration of ten minutes, followed by a period of 4 h for settling. The resulting solid materials were successively rinsed with ethanol and methanol, and then subjected to drying in an oven set at a temperature of 70 °C for a period of 12 h. The product was calcined in Ar atmosphere at

800 °C for 2 h, and after cooling, CoFe/Co@NC can be obtained. It was also compared with powders pyrolyzed at 600, 700, and 900 °C.

Characterization

The appearance of samples was analyzed using a field-emission scanning electron microscope (FESEM, acceleration voltage = 5 kV, SU-8010, HITACHI, Japan) and transmission electron microscope (TEM, acceleration voltage = 200 kV, FEI Talos F200x G2, America). Collect energy dispersive X-ray spectroscopy (EDS, Oxford, Xplore) using scanning electron microscopy (SEM) apparatus. The crystallographic phases of the samples were determined using an X-ray diffraction (XRD) analyzer (D8-Advance, Bruker, Germany) with a Cu-Kα radiation source (λ = 0.15406 nm, 40 kV, 30 mA). XRD patterns from five to 80 degrees were recorded at a scanning speed of two degrees min^{-1}. The graphitization degree of carbon in the sample was analyzed by a Raman spectrometer (LABRAM HR800, HORIBA). The laser wavelength was 532 nm. X-ray photoelectron spectroscopy (XPS, Thermo SCIENTIFIC Nexsa) was employed to study the chemical composition in the samples. Al Kα radiation was used as the X-ray source (1,486.68 eV) with a pass energy of 200 eV for survey spectra and 50 eV for high-resolution spectra. The energy resolution was 0.05 eV. XPS spectra were fitted using XPSpeak 4.1 software. The specific surface area of the samples was measured by the N_2 adsorption-desorption isotherms using the Brunauer-Emmett-Teller (BET) method. Barrett-Joyner-Halenda (BJH) strategy of Micromeritics (BRT, ASAP2020M, America) was used to evaluate the specific surface area and pore size.

Electromagnetic parameter analysis

The electromagnetic parameters of the sample were measured using a vector network analyzer (Agilent E5071C, USA) in the frequency range of 2-18 GHz. The product was mixed with paraffin to form an EMW absorption ring with an inner diameter of 3.04 mm and an outer diameter of 7.00 mm. The magnitude of R_L dictates the product's EMW absorption traits, and is calculated according to[21].

$$Z_{in} = Z_0(\mu_r/\varepsilon_r)^{1/2}\tanh[j(2\pi fd/c)(\varepsilon_r\mu_r)^{1/2}] \quad (1)$$

$$R_L = 20\log|(Z_{in} - Z_0)/(Z_{in} + Z_0)| \quad (2)$$

Here, Z_{in} and Z_0 were the input impedance and free-space impedance, respectively.

RESULTS AND DISCUSSION

A schematic diagram of CoFe/Co@NC heterostructure synthesis is shown in Figure 1. Firstly, porous CoFe-MOF cubes are prepared by chemical precipitation method at room temperature, in which Co and Fe ions are uniformly dispersed in the framework of the MOF. Then, during the calcination in Ar atmosphere, the MOF is reconfigured to form 2D NC nanosheets. At the same time, Co^{2+} and Fe^{2+} are converted into dual magnetic particles (0D CoFe alloy nanospheres and metallic Co hollow nanospheres), which are tightly embedded in 2D NC nanosheets to form rich heterogeneous interfaces (CoFe/NC, Co/NC). Furthermore, the heterostructure assembled from 2D NC nanosheets also provides opportunities for multiple reflections of EMWs.

From Supplementary Figure 1, it can be seen that the synthesized CoFe-MOF can be assigned to CoFe-ZIF, which is consistent with previous work[15]. CoFe/Co@NC shows crystalline phases of Co_3O_4 (PDF#42-1467) [Figure 2A], CoFe alloys (PDF#49-1567)[22], and metallic Co (PDF#15-0806)[23]. When the temperature is increased, the crystallinity of Co_3O_4 gradually decreases until the Co_3O_4 crystalline phase has completely disappeared at 900 °C. In contrast, the crystallinity of CoFe alloys first increases and then decreases with

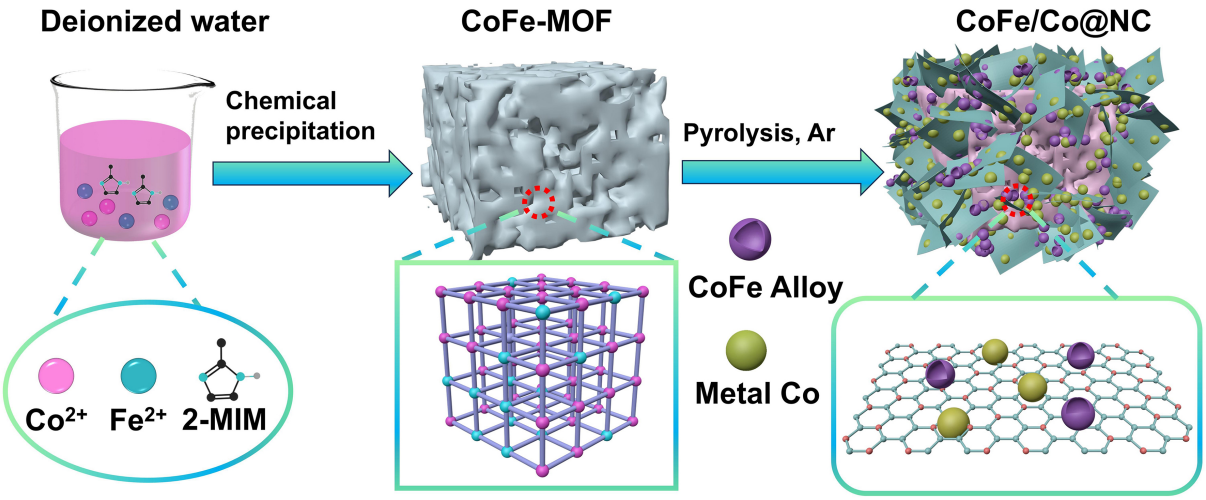

Figure 1. Schematic diagram of the synthesis process and corresponding microstructure CoFe/Co@NC heterostructure. NC: Nitrogen-doped carbon.

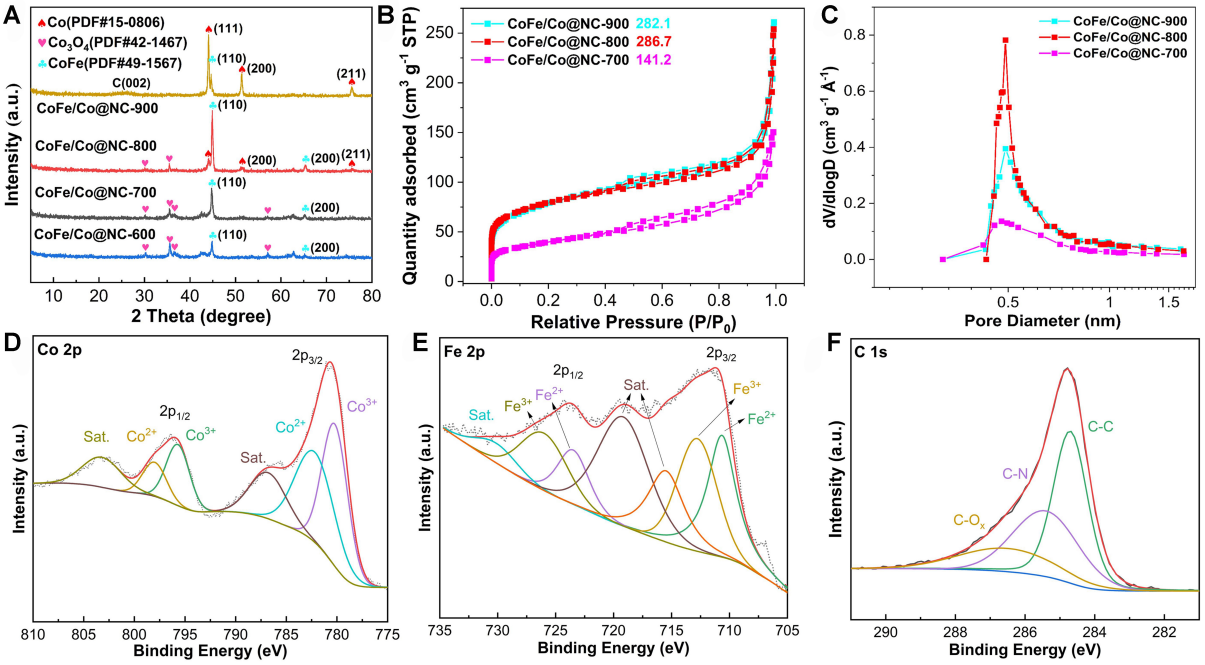

Figure 2. (A) XRD patterns and (B and C) N_2 adsorption-desorption isotherms of the samples. High-resolution XPS spectra of (D) Co 2p, (E) Fe 2p, and (F) C 1s. XRD: X-ray diffraction; XPS: X-ray photoelectron spectroscopy.

rising temperature. The diffraction peak at 45° is the (110) face of the CoFe alloy (PDF#49-1567), and the crystallinity of the CoFe alloy reaches its maximum value at 800 °C. At the same time, the crystalline phases of metallic Co also appear at 44°, 51°, and 75°, matching the (111), (200), and (211) crystal faces, respectively[24]. When the temperature reaches 900 °C, a distinct carbon peak appears around 26°[25]. It can also be seen that the crystallinity of Co is greater than that of CoFe alloys, which may also be the reason for the degradation of EMW absorption performance.

Figure 2B and C displays the N_2 adsorption-desorption isotherms of CoFe/Co@NC obtained through pyrolysis at varying temperatures. The relative pressure (P/P_0) of the isotherms for the samples ranges from 0.4 to 1.0, exhibiting typical type IV curves with hysteresis loops, indicating that the CoFe/Co@NC inherits a porous structure[26]. In terms of specific surface area, the samples pyrolyzed at 800 and 900 °C are much higher than those pyrolyzed at 700 °C. The specific surface areas of CoFe/Co@NC obtained by pyrolysis at 700, 800 and 900 °C are 141.2, 286.7 and 282.1 $m^2 \cdot g^{-1}$, respectively [Figure 2B], which is beneficial to expanding the consumption path of EMWs. Furthermore, their pore sizes are 0.47, 0.49 and 0.49 nm, respectively [Figure 2C].

To study the chemical composition of CoFe/Co@NC, the samples are analyzed by XPS. As shown in Supplementary Figure 2, the atomic content of elements such as Co, Fe, N, C and O in CoFe/Co@NC are 8.16%, 4.79%, 5.82%, 52.14%, and 29.09%, respectively. As shown in Figure 2D and E, due to spin-orbital splitting, the 2p spectra of Co and Fe correspond to the XPS spectra of $2P_{1/2}$ and $2p_{3/2}$ parts. The XPS spectra of Co 2p show six peaks at 780.4, 785.6, 783.6 and 795.4 eV, which correspond to Co^{3+} $2p_{3/2}$, Co^{3+} $2p_{1/2}$, Co^{2+} $2p_{3/2}$ and Co^{2+} $2p_{1/2}$, respectively[27]. In XPS spectra of Fe 2p, the peaks at 710.6 and 724.6 eV are Fe^{2+} peaks, the peaks at 713.0 and 726.8 eV correspond to Fe^{3+} peaks, and two satellite peaks are at 719.1 and 731.0 eV[28]. The XPS spectra of C 1s show that there are C-C (284.7 eV), C-N (285.4 eV) and C-O_x groups (286.5 eV) [Figure 2F][29]. The results indicate that N successfully doped carbon, which can induce dipole polarization due to its different electronegativity compared to carbon atoms. In addition, the XPS spectra of N 1s show three peaks: pyridine N (398.5 eV), pyrrolic N (399.7 eV), and graphite N (401.1 eV) [Supplementary Figure 3][30].

The structure and appearance of the samples are observed through SEM and TEM, as presented in Figure 3. Initially, CoFe-MOF shows a cubic structure with a size of ~1.6 μm, and the cube shows porous and has a rough surface [Figures 3A and Supplementary Figure 4]. After pyrolysis, the cubic block underwent structural reconstruction to generate 2D nanosheets, on which many 0D nanospheres with a diameter of ~30 nm are embedded [Figure 3B and Supplementary Figure 5]. This not only provides rich interfaces, but also expands the multiple reflection paths of EMWs. Furthermore, a large number of metal nanospheres also experience eddy current losses, thereby enhancing magnetic losses. Compounding dielectric carbon with magnetic particles can boost the impedance matching of the heterostructure, thereby enhancing the EMW absorption capability of CoFe/Co@NC. The elemental mapping image of CoFe/Co@NC is shown in Supplementary Figure 6, indicating that the Co, Fe, N, and C elements are uniformly distributed in the whole structure. From the TEM images in Figure 3C and D, and Supplementary Figure 7, it can be clearly observed that these nanoparticles are divided into two types: solid nanospheres wrapped with carbon and hollow nanospheres with a shell thickness of ~5 nm. In high-resolution TEM (HRTEM) [Figure 3D and F], the solid nanospheres have a lattice distance of 0.20 nm, which can correspond to the (111) face of Co. The hollow nanospheres exhibit a lattice distance of 0.21 nm, matching with the (110) face of CoFe alloys. These results confirm the formation of dual magnetic particles (Co and CoFe alloys) in the heterostructures.

According to the electromagnetic parameters, the 2D and 3D R_L curves of the specimens are shown in Figure 4. Figure 4A and E shows the R_L curve of CoFe/Co@NC-600, which does not show effective EMW absorption. When the pyrolysis temperature rises to 700 °C, the obtained CoFe/Co@NC-700 displays R_L of -29.13 dB at a thickness of 5 mm [Figure 4B and F]. Especially when the pyrolysis temperature is 800 °C, the CoFe/Co@NC-800 achieves very strong R_L (-73.8 dB, 99.999%) at an ultrathin matching thickness of 1.78 mm [Figure 4C and G]. The EAB reaches 5.4 GHz. Importantly, EAB values for matching thickness between 1-5 mm are 14.73 GHz (3.27-18 GHz, covering the whole C, X, Ku frequency bands and most S bands), comprising 92% of the test frequencies (2-18 GHz). As the temperature increases, the improvement

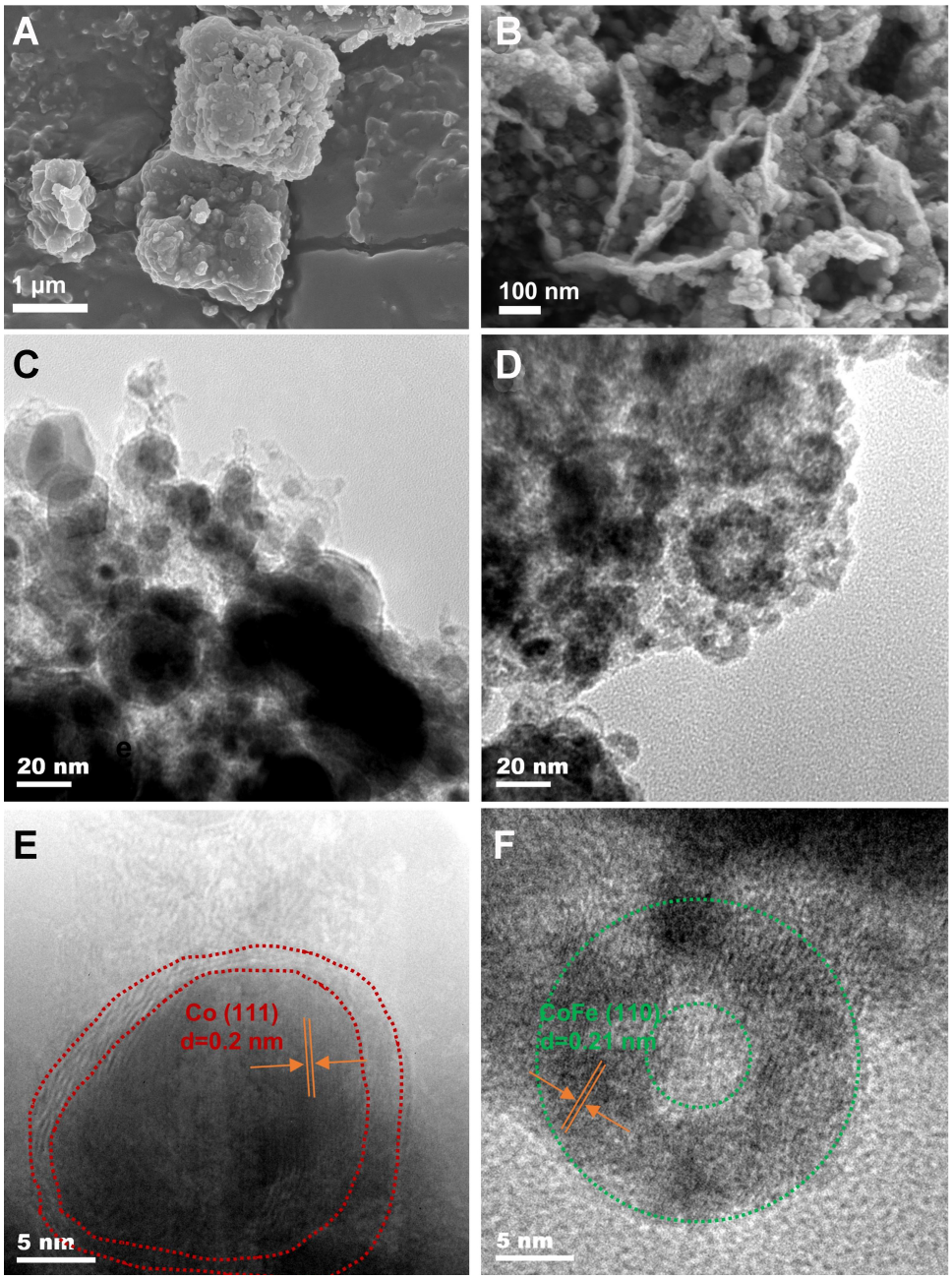

Figure 3. SEM images of (A) CoFe-MOF and (B) CoFe/Co@NC. (C and D) TEM and (E and F) HRTEM images of CoFe/Co@NC. SEM: Scanning electron microscopy; MOF: metal-organic framework; NC: nitrogen-doped carbon; TEM: transmission electron microscope; HRTEM: high-resolution TEM.

of properties is due to the increase in CoFe alloy content, which further enhances the magnetic loss of the heterostructure, thus enhancing the absorption capacity of EMW. Meanwhile, the continuous formation of nanosheets and hollow nanospheres also enhances the multiple reflections of incident EMW. However, as the pyrolysis temperature rises to 900 °C, the R_L is very low [Figure 4D and H], which may be due to the reduction of CoFe alloy content, as shown in the XRD results.

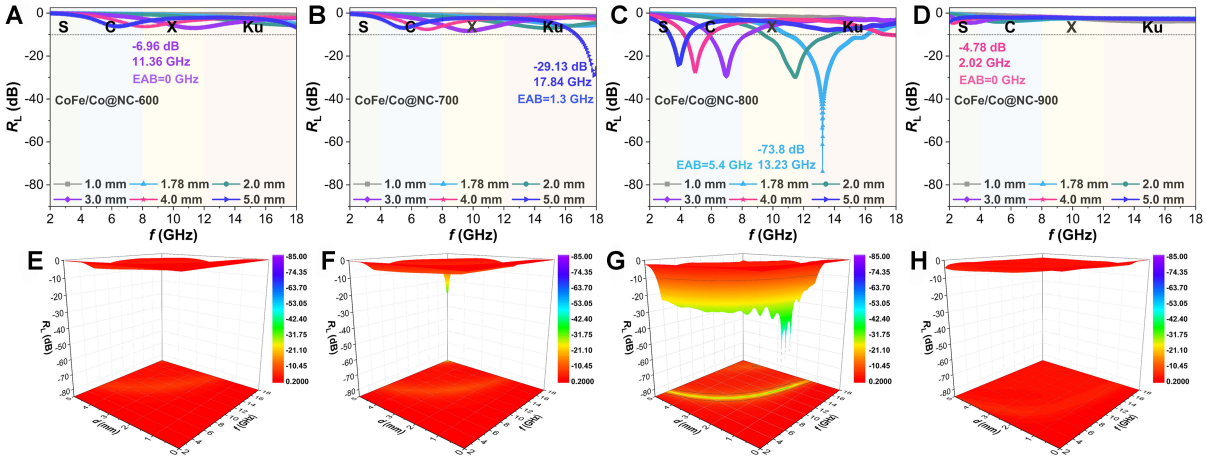

Figure 4. (A-D) 2D and (E-H) 3D R_L curves of CoFe/Co@NC pyrolyzed at (A and E) 600, (B and F) 700, (C and G) 800, and (D and H) 900 °C. NC: Nitrogen-doped carbon.

To further investigate the outstanding EMW absorption capacity of CoFe/Co@NC heterostructures, the complex permittivity ($\varepsilon_r = \varepsilon' - j\varepsilon''$) and complex permeability ($\mu_r = \mu' - j\mu''$) are discussed[31]. ε' can show the storage capacity of the material, and ε'' can represent the EMW loss capacity[32,33]. According to the theory of electronic degrees of freedom, a high ε'' indicates a high dielectric conductivity, which leads to strong EMW reflection and is not conducive to impedance matching[34,35]. Therefore, the highest ε' and ε'' values of CoFe/Co@NC-900 reflect its poor EMW absorption capacity [Figure 5A and B]. In contrast, CoFe/Co@NC-800 exhibits moderate ε' and ε'' values, which balance the magnetic permeability and promote the EMW absorption. tan $\delta_\varepsilon = \varepsilon''/\varepsilon'$ is considered as dielectric loss, which represents the attenuation ability of electric energy. As can be seen from Figure 5C, although CoFe/Co@NC-900 has the largest dielectric loss, due to its strong reflection, there are few incident EMWs, resulting in poor performance. The dielectric loss value of CoFe/Co@NC-800 is moderate, which corresponds to its outstanding EMW absorption capacity. Same as the permittivity, μ' indicates the storage and μ'' indicates the loss of magnetic energy[36,37]. CoFe/Co@NC-800 enables the largest μ' value, illustrating that it has the largest magnetic energy storage capacity [Figure 5D]. Generally, in the μ'' curve, the peak at low frequency is natural resonance, and the peak at high frequency represents exchange resonance[38,39]. The high-frequency domain displays resonance peaks for CoFe/Co@NC-800, signifying the occurrence of exchange resonance. In addition, the value of μ'' becomes negative in the high-frequency region (14-17 GHz) [Figure 5E], mainly due to the built-in electric field generating a magnetic field opposite to the incident EMW. When the material has high electrical conductivity, it will generate a magnetic field to cancel the external magnetic field, thus suppressing magnetic losses and resulting in negative μ'' values. Furthermore, tan $\delta_\mu = \mu''/\mu'$ is considered as magnetic loss, which represents the attenuation ability of magnetic energy[40]. The magnetic loss of magnetic nanoparticles usually has three factors, namely natural resonance, exchange resonance, and eddy current loss[41]. In the whole measuring frequency range, the tan δ_ε value of CoFe/Co@NC-800 is higher than its tan δ_μ value [Figure 5F], indicating that dielectric loss is the main factor of EMW attenuation.

Based on Debye's theory, the Cole-Cole diagram can be used to determine the polarization process, and the relationship between ε' and ε'' can be expressed by $(\varepsilon' - \varepsilon_\infty)^2 + (\varepsilon'')^2 = (\varepsilon_s - \varepsilon_\infty)^2$[42]. When Debye relaxation occurs, the corresponding Cole-Cole curve will have a semicircle followed by a straight line. The semicircle represents polarization loss, and the straight line represents conduction loss; the more semicircles there are, the stronger the polarization relaxation[43]. CoFe/Co@NC-600 has fewer semicircles and no straight lines [Figure 6A], indicating that their dielectric loss capability is poor. Although CoFe-NC-700 has both

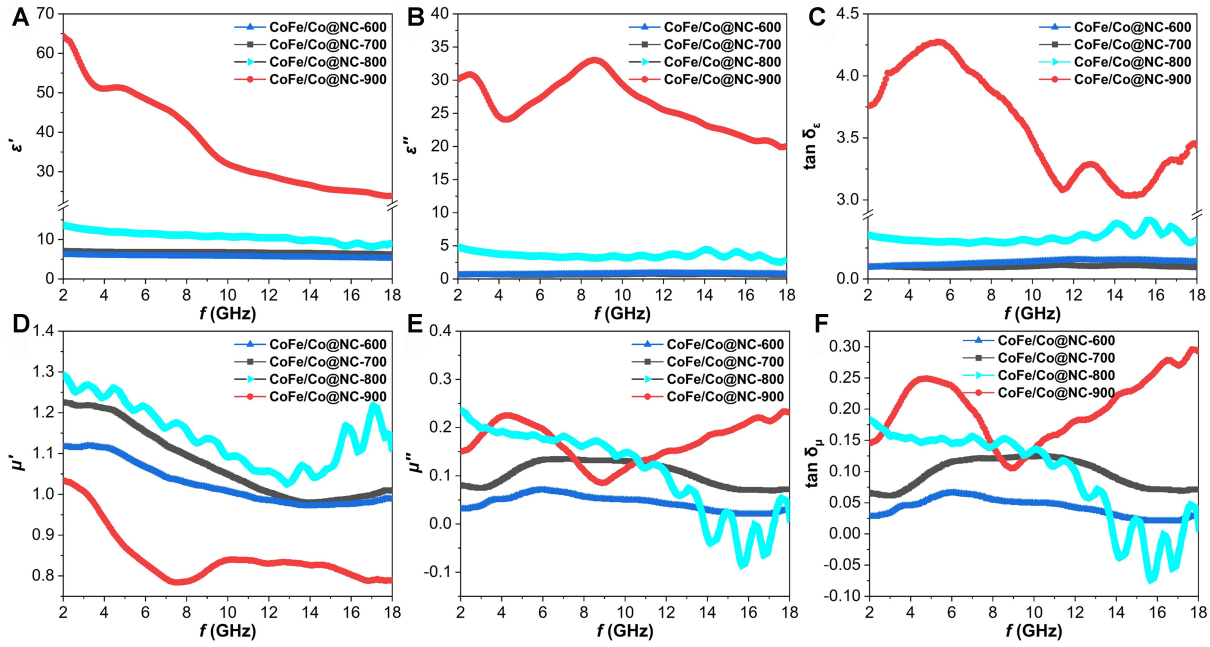

Figure 5. (A) ε', (B) ε'', (C) tan δ_{ε}, (D) μ', (E) μ'', and (F) tan δ_{μ} values of the samples.

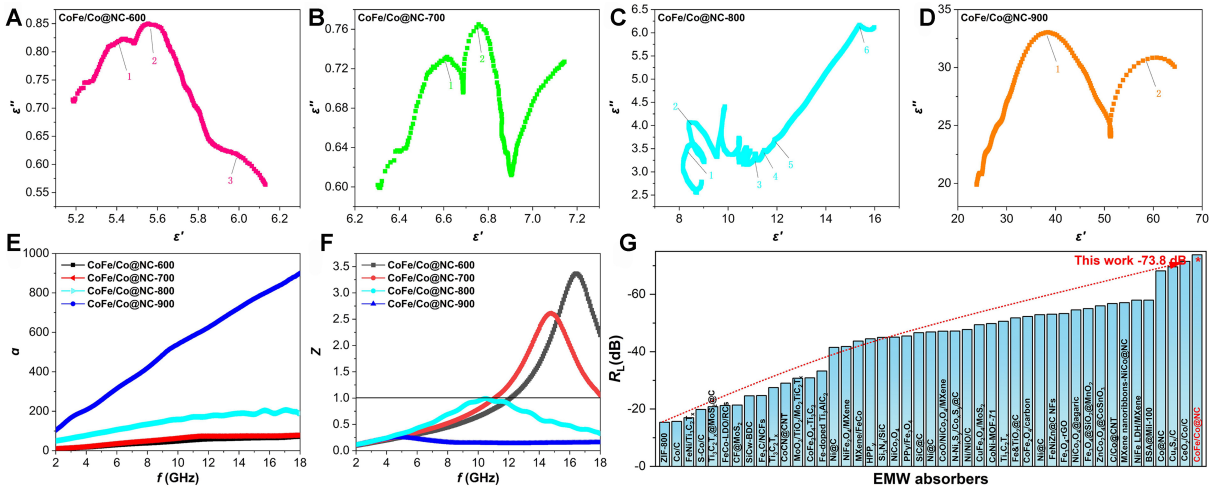

Figure 6. (A-D) Cole-Cole curves of CoFe/Co@NC pyrolyzed at different temperatures. (E) Z and (F) α worth of the samples. (G) Comparison of the EMW absorption capacity of CoFe/Co@NC and reported excellent absorbers. NC: Nitrogen-doped carbon; EMW: electromagnetic wave.

semicircles and straight lines [Figure 6B], it only has two semicircles, so its polarization loss capability is relatively low. Notably, the Cole-Cole diagram of CoFe/Co@NC-800 is also composed of semicircles and straight lines [Figure 6C], but there are more semicircles, which indicates that it has strong polarization loss and conductivity loss. In contrast, CoFe/Co@NC-900 has fewer semicircles and no straight lines, as shown in Figure 6D.

The EMW absorption capacity of the samples directly depends on the reflection and attenuation of incident EMWs. Reflection is related to impedance matching, while attenuation is related to electromagnetic losses. When Z value ($Z = (\mu_r/\varepsilon_r)^{1/2}\tanh|j2\pi fd(\mu_r\varepsilon_r)^{1/2}/c|$) is close to 1, it indicates that the impedance matching is

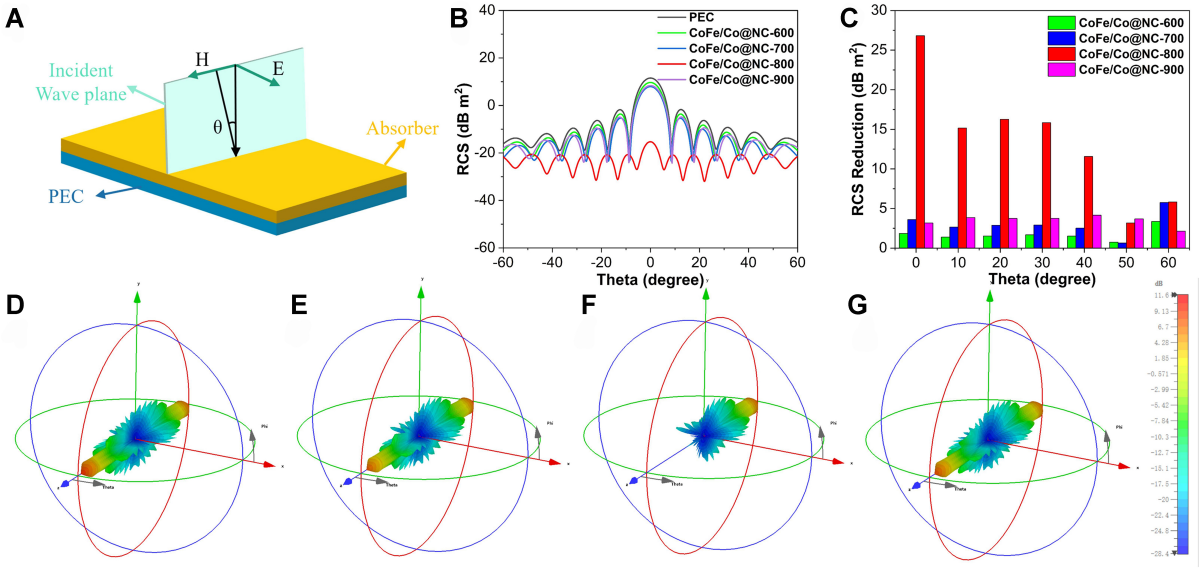

Figure 7. (A) RCS Simulation model; (B) RCS curves and (C) RCS decrease values of samples; CST simulation results of (D) CoFe/Co@NC-600, (E) CoFe/Co@NC-700, (F) CoFe/Co@NC-800, and (G) CoFe/Co@NC-900 heterostructures. RCS: Radar cross section; CST: computer simulation technology; NC: nitrogen-doped carbon.

good[44]. As shown in Figure 6E, the *Z* worth of CoFe/Co@NC-800 is about 1, corresponding to its best EMW absorption performance. CoFe/Co@NC-900 shows impedance mismatch due to excessively high ε' and ε" values. In addition, the attenuation constant ($\alpha = [((2)^{1/2}\pi f)/c]/\{(\mu"\varepsilon" - \mu'\varepsilon') + [(\varepsilon'\mu" + \varepsilon"\mu')^2 + (\mu"\varepsilon" - \mu'\varepsilon')^2]^{1/2}\}^{1/2}$) is utilized to assess the attenuation ability of EMW[45-47]. Theoretically, the larger the α value, the better. As shown in Figure 6F, CoFe/Co@NC-900 shows the largest α value, but reflects numerous EMWs due to its impedance mismatch. In addition, the α worth of CoFe/Co@NC-800 is higher than that of CoFe/Co@NC-600 and CoFe/Co@NC-700, so it has outstanding EMW absorption capacity. The outstanding EMW absorption of CoFe/Co@NC makes it one of the excellent EMW absorbers, as shown in Figure 6G and Supplementary Table 1.

Simulation of the RCS for the sample using CST software allows for better investigation of the potential of CoFe/Co@NC in practical applications[48]. Figure 7A shows the RCS simulation model, in which the positive direction of the Z-axis and θ represent the incident orientation and detection angle. For the reflected signals, the smaller the RCS worth, the stronger the EMW absorption capacity[49,50]. Figure 7B shows the 2D RCS worth of the sample obtained through simulation at different scattering angles. Obviously, the RCS value of CoFe/Co@NC-800 is the smallest in the range of -60° to 60°. To more clearly illustrate the influence of the EMW absorption layer on RCS decrease, Figure 7C shows the RCS decrease value calculated through the differential method, with seven detection angles set. For CoFe/Co@NC-800, the maximum RCS reduction is observed at 0°. Figure 7D-G shows the 3D radar wave scattering patterns for the PEC and various samples. It can be observed that CoFe/Co@NC-800 with PEC coverage has the lowest scattering intensity. These results correspond to R_L values, further confirming that CoFe/Co@NC-800 has strong radar stealth potential.

Based on the above phase, structure, and performance analysis, we proposed the EMW absorption mechanism of CoFe/Co@NC heterostructure, as shown in Figure 8. Many solid and hollow magnetic nanospheres are embedded in dielectric nanosheets to effectively adjust the impedance matching. The good impedance-matching characteristics of the CoFe/Co@NC heterostructure promote the entry of EMWs into

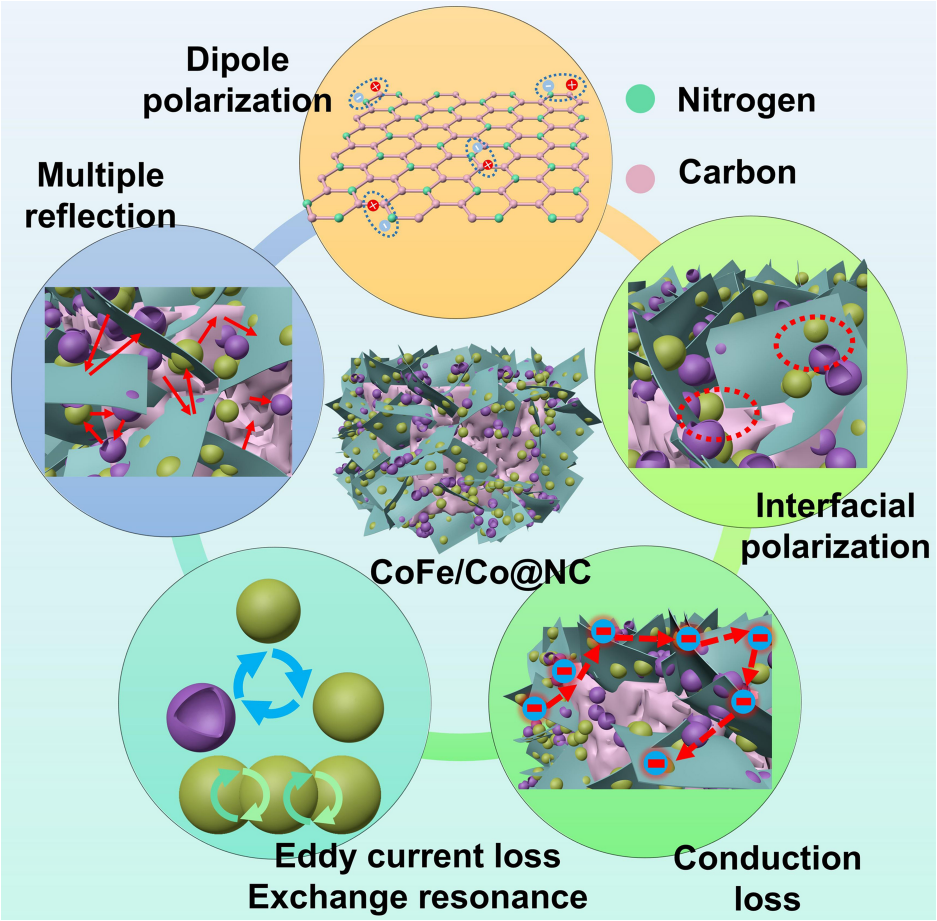

Figure 8. EMW absorption mechanism diagram of CoFe/Co@NC heterostructure. EMW: Electromagnetic wave; NC: nitrogen-doped carbon.

its interior. Due to the multiple reflections and scattering between its large number of nanosheets[51,52], the transmission path of EMWs is greatly increased, thereby enhancing EMW attenuation. Many heterogeneous interfaces are formed between hollow CoFe alloy nanospheres and NC nanosheets, metallic Co nanospheres and NC nanosheets, nanosheets and cube blocks, which will lead to significant interface polarization. Furthermore, many NC nanosheets are assembled to form a 3D conductive network, thereby enhancing the conduction loss in the absorber. Electron migration and jumping between nanospheres and between nanospheres also contribute to conduction losses. At the same time, the electronegativity of N heteroatoms is different from that of C atoms, so doping numerous N atoms in the carbon matrix will induce dipole polarization. Combining these dielectric behaviors, CoFe/Co@NC exhibits outstanding dielectric loss characteristics. On the other hand, the abundant magnetic nanospheres in the heterostructure promote the exhibition of exchange resonance characteristics. Many adjacent nanospheres also generate eddy current losses, which enhance the magnetic loss characteristics. Therefore, CoFe/Co@NC heterostructure has outstanding EMW absorption performance due to the synergistic effect of interfacial polarization, multiple reflections, conduction loss, dipole polarization, exchange resonance and eddy current loss.

CONCLUSIONS

In summary, we demonstrate porous CoFe/Co@NC heterostructures derived from CoFe-MOF, in which dual magnetic particles (0D solid Co nanospheres and hollow CoFe nanospheres) embedded on 2D NC nanosheets through a simple chemical precipitation method and pyrolysis process. By regulating the pyrolysis temperature, the balance of dual magnetic particle (CoFe, Co) content is achieved, resulting in good impedance matching characteristics. The large number of heterogeneous interfaces, good conductive networks and multi-component magnetic nanoparticles in the CoFe/Co@NC heterostructure bring considerable interface polarization, conduction loss, and magnetic loss characteristics, thereby achieving robust EMW absorption performance. When the matching thickness is only 1.78 mm, the CoFe/Co@NC heterostructure achieves a very strong R_L (-73.8 dB) and a wide EAB of 5.4 GHz. CST simulations confirm the potential of CoFe/Co@NC heterostructures in radar stealth. This work provides a solid foundation for dual magnetic particles to achieve magnetoelectric synergy for the improvement of EMW absorption at ultrathin thickness.

DECLARATIONS

Authors' contributions

Data curation, investigation, methodology, software, writing - original draft, writing - review and editing: Wu Z

Software, Writing - review and editing: Huang J

Conceptualization, funding acquisition, project administration, resources, supervision, writing - original draft, writing - review and editing: Zeng X

Availability of data and materials

The data presented in this study is available upon request from the corresponding author.

Financial support and sponsorship

This work was supported by the National Natural Science Foundation of China (No. 22269010), the Jiangxi Provincial Natural Science Foundation (No. 20224BAB214021), and the Major Research Program of Jingdezhen Ceramic Industry (No. 2023ZDGG002).

Conflicts of interest

All authors declared that there are no conflicts of interest.

Ethical approval and consent to participate

Not applicable.

Consent for publication

Not applicable.

REFERENCES

1. Cheng J, Zhang H, Wang H, et al. Tailoring self-polarization of bimetallic organic frameworks with multiple polar units toward high-performance consecutive multi-band electromagnetic wave absorption at gigahertz. *Adv Funct Mater* 2022;32:2201129. DOI
2. Zhong X, He M, Zhang C, Guo Y, Hu J, Gu J. Heterostructured BN@Co-C@C endowing polyester composites excellent thermal conductivity and microwave absorption at C band. *Adv Funct Mater* 2024;34:2313544. DOI
3. Fang G, Liu C, Xu M, et al. The elaborate design of multi-polarization effect by non-edge defect strategy for ultra-broad microwave absorption. *Adv Funct Mater* 2024;34:2404532. DOI

4. Wang YQ, Zhao HB, Cheng JB, Liu BW, Fu Q, Wang YZ. Hierarchical $Ti_3C_2T_x$@ZnO hollow spheres with excellent microwave absorption inspired by the visual phenomenon of eyeless urchins. *Nanomicro Lett* 2022;14:76. DOI PubMed PMC
5. Yi P, Zou H, Yu Y, et al. MXene-reinforced liquid metal/polymer fibers via interface engineering for wearable multifunctional textiles. *ACS Nano* 2022;16:14490-502. DOI
6. Zeng X, Peng X, Ning Y, Jiang X, Yu R, Zhang X. 3D multifunctional porous pine carbon aerogels coupled with highly dispersed CoFe nanoparticles for robust electromagnetic wave response. *J Mater Sci Technol* 2024;192:6-18. DOI
7. He M, Hu J, Yan H, et al. Shape anisotropic chain-like CoNi/polydimethylsiloxane composite films with excellent low-frequency microwave absorption and high thermal conductivity. *Adv Funct Mater* ;2024:2316691. DOI
8. Guo Z, Lan D, Jia Z, et al. Multiple tin compounds modified carbon fibers to construct heterogeneous interfaces for corrosion prevention and electromagnetic wave absorption. *Nanomicro Lett* 2024;17:23. DOI PubMed PMC
9. Yan J, Zheng Q, Wang SP, et al. Multifunctional organic-inorganic hybrid perovskite microcrystalline engineering and electromagnetic response switching multi-band devices. *Adv Mater* 2023;35:e2300015. DOI
10. Zeng X, Zhao C, Nie T, Shen Z, Yu R, Stucky G. Construction of 0D/1D/2D MXene nanoribbons-NiCo@NC hierarchical network and their coupling effect on electromagnetic wave absorption. *Mater Today Phys* 2022;28:100888. DOI
11. Wu N, Yang Y, Wang C, et al. Ultrathin cellulose nanofiber assisted ambient-pressure-dried, ultralight, mechanically robust, multifunctional MXene aerogels. *Adv Mater* 2023;35:e2207969. DOI
12. Xiao J, Zhan B, He M, et al. Interfacial polarization loss improvement induced by the hollow engineering of necklace-like PAN/carbon nanofibers for boosted microwave absorption. *Adv Funct Mater* ;2024:2316722. DOI
13. Zhao C, Zeng X, Huang J, Gao Y, Fan B. MXene-derived titanate heterojunctions with lightweight and heat-resistant properties for electromagnetic wave absorption. *Carbon* 2024;228:119422. DOI
14. Wu Y, Tan S, Fang G, Zhang Y, Ji G. Manipulating CNT films with atomic precision for absorption effectiveness–enhanced electromagnetic interference shielding and adaptive infrared camouflage. *Adv Funct Mater* ;2024:2402193. DOI
15. Guo S, Bao Y, Li Y, et al. Super broadband absorbing hierarchical CoFe alloy/porous carbon@carbon nanotubes nanocomposites derived from metal-organic frameworks. *J Mater Sci Technol* 2022;118:218-28. DOI
16. He M, Lv X, Peng H, et al. Biomimetic artificial nacre-like microfiber of Co/C modified cellulose nanofiber/$Ti_3C_2T_x$ MXene with efficient microwave absorption. *Chem Eng J* 2024;491:151726. DOI
17. Wen B, Yang H, Lin Y, Qiu Y, Cheng Y, Jin L. Novel bimetallic MOF derived hierarchical Co@C composites modified with carbon nanotubes and its excellent electromagnetic wave absorption properties. *J Colloid Interface Sci* 2022;605:657-66. DOI
18. Jin L, Yi P, Wan L, et al. Thickness-controllable synthesis of MOF-derived Ni@N-doped carbon hexagonal nanoflakes with dielectric-magnetic synergy toward wideband electromagnetic wave absorption. *Chem Eng J* 2022;427:130940. DOI
19. Zhu H, Jiao Q, Fu R, et al. Cu/NC@Co/NC composites derived from core-shell Cu-MOF@Co-MOF and their electromagnetic wave absorption properties. *J Colloid Interface Sci* 2022;613:182-93. DOI
20. Wang Y, Wang H, Ye J, Shi L, Feng X. Magnetic CoFe alloy@C nanocomposites derived from ZnCo-MOF for electromagnetic wave absorption. *Chem Eng J* 2020;383:123096. DOI
21. Zeng X, Jiang X, Ning Y, Hu F, Fan B. Construction of dual heterogeneous interface between zigzag-like Mo–MXene nanofibers and small CoNi@NC nanoparticles for electromagnetic wave absorption. *J Adv Ceram* 2023;12:1562-76. DOI
22. Wang C, Zeng X, Jiang G, Chen M, Zhu L, Yu R. General self-template synthesis of transition-metal oxide microspheres and their excellent charge storage properties. *Electrochim Acta* 2018;283:190-6. DOI
23. Zeng X, Jang MJ, Choi SM, Cho HS, Kim CH, Myung NV, Yin Y. Single-crystalline CoFe nanoparticles encapsulated in N-doped carbon nanotubes as a bifunctional catalyst for water splitting. *Mater Chem Front* 2020;4:2307-13. DOI
24. Lv H, Liang X, Ji G, Zhang H, Du Y. Porous three-dimensional flower-like Co/CoO and its excellent electromagnetic absorption properties. *ACS Appl Mater Interfaces* 2015;7:9776-83. DOI
25. Liu P, Huang Y, Yan J, Yang Y, Zhao Y. Construction of CuS nanoflakes vertically aligned on magnetically decorated graphene and their enhanced microwave absorption properties. *ACS Appl Mater Interfaces* 2016;8:5536-46. DOI
26. Kong F, Chen K, Song S, Xue D. Metal organic framework derived CoFe@N-doped carbon/reduced graphene sheets for enhanced oxygen evolution reaction. *Inorg Chem Front* 2018;5:1962-6. DOI
27. Huang W, Ma H, Qi J, et al. Electron-deficient Co_7Fe_3 induced by interfacial effect of molybdenum carbide boosting oxygen evolution reaction. *J Colloid Interface Sci* 2024;669:95-103. DOI PubMed
28. Meng Y, Huang Y, Huang G, Song Y. TPN-COF@Fe-MIL-100 composite used as an electrochemical aptasensor for detection of trace tetracycline residues. *RSC Adv* 2023;13:28148-57. DOI PubMed PMC
29. Kononenko O, Brzhezinskaya M, Zotov A, et al. Influence of numerous Moiré superlattices on transport properties of twisted multilayer graphene. *Carbon* 2022;194:52-61. DOI
30. Brzhezinskaya M, Mishakov IV, Bauman YI, et al. One-pot functionalization of catalytically derived carbon nanostructures with heteroatoms for toxic-free environment. *Appl Surf Sci* 2022;590:153055. DOI
31. He M, Chen H, Peng H, et al. Ultralight $Ti_3C_2T_x$-derivative chrysanthemum-like $Na_2Ti_3O_7/Ti_3C_2T_x$ MXene quantum dots 3D/0D heterostructure with advanced microwave absorption performance. *Chem Eng J* 2023;456:140985. DOI
32. Zeng X, Nie T, Zhao C, Gao Y, Liu X. In situ exsolution-prepared solid-solution-type sulfides with intracrystal polarization for efficient and selective absorption of low-frequency electromagnetic wave. *Adv Sci* 2024;11:e2403723. DOI PubMed PMC
33. Zhang Q, Lan D, Deng S, et al. Constructing multiple heterogeneous interfaces in one-dimensional carbon fiber materials for superior

electromagnetic wave absorption. *Carbon* 2024;226:119233. DOI

34. Ning Y, Jiang X, Huang J, Gao Y, Zeng X. Trimetallic MOFs derived $NiFe_2O_4$/$MoNi_4$-NC Schottky heterojunctions with abundant defects and dielectric-magnetic coupling for electromagnetic response. *J Mater Sci Technol* 2025;213:1-13. DOI
35. Zhao Y, He Q, Liu M, et al. Combustion-assisted construction of defect-enriched hierarchical carbon composites towards efficient low-frequency electromagnetic wave absorption. *Chem Eng J* 2024;488:150893. DOI
36. Zeng X, Zhao C, Yin Y, et al. Construction of $NiCo_2O_4$ nanosheets-covered $Ti_3C_2T_x$ MXene heterostructure for remarkable electromagnetic microwave absorption. *Carbon* 2022;193:26-34. DOI
37. Sun C, Lan D, Jia Z, Gao Z, Wu G. Kirkendall effect-induced ternary heterointerfaces engineering for high polarization loss MOF-LDH-MXene absorbers. *Small* 2024;20:e2405874. DOI PubMed
38. Zhao Y, Wang N, Wang H, et al. Chiral structure induces spatial spiral arrangement of Fe_3O_4 nanoparticles to optimize electromagnetic wave dissipation. *Appl Phys Lett* 2024;124:161901. DOI
39. Wu D, Lan D, Li Y, Zhou N, He Q, Wang Y. Heterostructure engineering of N-doped Co@ carbon nanotubes toward broadband efficient electromagnetic absorption. *Colloid Surface A* 2024;702:135161. DOI
40. Zeng X, Zhao C, Jiang X, Yu R, Che R. Functional tailoring of multi-dimensional pure MXene nanostructures for significantly accelerated electromagnetic wave absorption. *Small* 2023;19:e2303393. DOI
41. Zhao T, Lan D, Jia Z, Gao Z, Wu G. Hierarchical porous molybdenum carbide synergic morphological engineering towards broad multi-band tunable microwave absorption. *Nano Res* 2024;17:9845-56. DOI
42. Liu Y, Wei X, He X, et al. Multifunctional shape memory composites for joule heating, self-healing, and highly efficient microwave absorption. *Adv Funct Mater* 2023;33:2211352. DOI
43. Xie A, Ma Z, Xiong Z, et al. Conjugate ferrocene polymer derived magnetic Fe/C nanocomposites for electromagnetic absorption application. *J Mater Sci Technol* 2024;175:125-31. DOI
44. Pan F, Shi Y, Yang Y, et al. Porifera-inspired lightweight, thin, wrinkle-resistance, and multifunctional MXene foam. *Adv Mater* 2024;36:e2311135. DOI
45. Zeng X, Li E, Xia G, et al. Silica-based ceramics toward electromagnetic microwave absorption. *J Eur Ceram Soc* 2021;41:7381-403. DOI
46. Zhan B, Qu Y, Qi X, et al. Mixed-dimensional assembly strategy to construct reduced graphene oxide/carbon foams heterostructures for microwave absorption, anti-corrosion and thermal insulation. *Nanomicro Lett* 2024;16:221. DOI PubMed PMC
47. Zeng X, Jiang X, Ning Y, Gao Y, Che R. Constructing built-in electric fields with semiconductor junctions and schottky junctions based on Mo-MXene/Mo-metal sulfides for electromagnetic response. *Nanomicro Lett* 2024;16:213. DOI PubMed PMC
48. Liang H, Chen G, Liu D, et al. Exploring the Ni 3*d* orbital unpaired electrons induced polarization loss based on Ni single-atoms model absorber. *Adv Funct Mater* 2023;33:2212604. DOI
49. Zhai N, Luo J, Mei J, et al. Interface engineering of heterogeneous $NiSe_2$-$CoSe_2$ @C@$MoSe_2$ for high-efficient electromagnetic wave absorption. *Adv Funct Mater* 2024;34:2312237. DOI
50. Ning Y, Zeng X, Peng X, et al. Dual template-derived 3D porous $Co_6Mo_6C_2$/Mo_2C@NC framework for electromagnetic wave response and multifunctional applications. *J Mater Sci Technol* 2024;187:15-27. DOI
51. Yu H, Kou X, Zuo X, et al. Optimization of multiple attenuation mechanisms by cation substitution in imidazolic MOFs-derived porous composites for superior broadband electromagnetic wave absorption. *J Mater Sci Technol* 2024;176:176-87. DOI
52. Pan F, Pei K, Chen G, et al. Integrated electromagnetic device with on-off heterointerface for intelligent switching between wave-absorption and wave-transmission. *Adv Funct Mater* 2023;33:2306599. DOI